

NbC-BASED CERMET PRODUCTION COMPARISON: L-PBF ADDITIVE MANUFACTURING VERSUS CONVENTIONAL LPS POWDER METALLURGY

PROIZVODNJA KERMETOV NA OSNOVI NBC; PRIMERJAVA MED DODAJALNO TEHNOLOGIJO L-PBF IN KONVENCIONALNO METALURGIJO PRAHOV LPS

Fabio Miranda^{1,3*}, Marcelo Otavio dos Santos^{1,2}, Daniel Rodrigues³,
Rodrigo Santiago Coelho⁴, Gilmar Ferreira Batalha¹

¹University of São Paulo, Polytechnic School, EPUSP-PMR, São Paulo, Brazil

²Mauá Institute of Technology, University Centre, São Caetano do Sul, Brazil

³BRATS Sintered Filters and Metallic Powders, Cajamar-SP, Brazil

⁴SENAI CIMATEC – Institute of Innovation for Forming & Joining of Materials, Salvador, Bahia, Brazil

Prejem rokopisa – received: 2023-01-30; sprejem za objavo – accepted for publication: 2023-08-28

doi:10.17222/mit.2023.972

The production of carbide parts (cermet) by additive manufacturing, such as laser powder bed fusion (L-PBF), has been a great challenge due to the complex optimization of process parameters to improve density, porosity, microcracks or abnormal growth of grains and obtain a microstructure as homogeneous as possible. This work aims to compare the evolution of the microstructure when using the conventional route of powder metallurgy, i.e., liquid phase sintering (LPS) with the L-PBF direct additive manufacturing process, considering the NbC-based carbide material. Sample compositions were prepared in w%, samples were compacted under 50–125 MPa, without polymeric binders, and they were sintered under a vacuum at temperatures of 1330 °C and 1370 °C. For the L-PBF process, a vibrating device made it possible to improve the fluidity of the mixtures of three alloys, NbC–30Co, NbC–30Ni and NbC–30(Co, Ni). The mixtures exhibited low sphericity, low fluidity and compressibility, which were improved with a roller compactor. Thin powder mixture deposition layers were evenly applied and well distributed across the powder bed to avoid defects and cracks during sintering. The L-PBF process parameters varied including a power of 50–125 W and a laser scanning speed of 25–125 mm·s⁻¹. Different microstructures, identified with a light microscope (LM) and a scanning electron microscope (SEM), and properties obtained with the two processes, direct (L–PBF) and indirect sintering (LPS), were compared.

Keywords: NbC–cemented carbides, L–PBF additive manufacturing, liquid phase sintering, microstructure and mechanical properties

Proizvodnja karbidnih trdin oziroma kompozitov na osnovi drobnih karbidnih delcev v kovinski osnovi (kermeti; kompoziti keramika-kovina) z dodajalno tehnologijo, kot je naprimer lasersko pretaljevanje nanosov plasti prahu za plastjo (L-PBF; angl.: Laser Powder Bed Fusion), je zelo zahtevno zaradi komplicirane optimizacije procesnih parametrov, ki naj izboljšajo gostoto, zmanjšajo poroznost in število mikrorazpok ali nenormalno (pretirano) rast kristalnih zrn in s tem zagotovijo čim bolj homogeno mikrostrukturo. V tem članku avtorji opisujejo primerjavo razvoja mikrostrukture karbidne trdine na osnovi NbC nastale s postopkom konvencionalne metalurgije prahov oz. postopkom sintranja v prisotnosti tekoče faze (LPS; angl.: Liquid Phase Sintering) z mikrostrukturo nastalo med direktnim L-PBF postopkom. Avtorji so surove vzorce za LPS pripravili s stiskanjem pri 50 MPa do 125 MPa brez dodatka polimernega veziva in jih sintrali v vakuumu pri temperaturah 1330 °C in 1370 °C. Za L-PBF postopek so uporabili vibracijsko napravo, ki je izboljšala tekočnost (nasipanje) treh izbranih prašnih mešanic: NbC-30Co, NbC-30Ni in NbC-30(Co, Ni). Te mešanice imajo delce dokaj neprevilne oblike in se zato slabo nasipavajo plast za plastjo. Izboljšanje zgoščevanja plasti so dosegli z dodatno uporabo valja (angl.: roller compactor). Tako so bile enakomerno nanešene tanke plasti prašnih mešanic z dobro porazdelitvijo prašnih delcev v posteljici, kar naj bi preprečilo nastajanje razpok in drugih napak med sintranjem. Parametre L-PBF procesa so varirali; moč med 50 W in 125 W ter skeniranje z laserjem s hitrostjo od 25 mm·s⁻¹ do 125 mm·s⁻¹. Nato so avtorji izvedli še primerjavo mikrostruktur in morfoloških lastnosti dobljenih z obema postopkoma (direktnim L-PBF in indirektnim LPS postopkom). Primerjave so izvedli s pomočjo svetlobnega oziroma optičnega (LM) in vrstičnega elektronskega mikroskopa (SEM).

Ključne besede: karbidne trdine na osnovi NbC, dodajalna tehnologija (L-PBF), sintranje v tekoči fazi (LPS), mikrostruktura in mehanske lastnosti

1 INTRODUCTION

New cermets based on NbC with alternative Ni binder phases and a Co/Ni combination, being face-centered cubic (FCC), emerged to minimize the consumption of traditional WC–Co alloys, mainly for the manufacture of cutting tools for machining subject to high

temperatures and wear resistance.¹ NbC_y (0.77 < y < 0.96) has been used as a secondary hard phase for high-speed steels and as an inhibitor for the WC grain growth for cermet tools, but its potential to be used as a primary hard phase needs to be further explored.³ Little attention was given to NbC in the 19th century, but recent studies have shown promising results, allowing us to replace WC with NbC, especially for cutting tools and wear resistance.^{1–4} An NbC-based cermet with an amount of

*Corresponding author's e-mail:
fabio.miranda@usp.br (Fabio Miranda)

combined carbon being above 10 w%, includes NbC + 12Ni + C (free), with its eutectic temperature close to 1265 °C, as seen on Figures 1a and 1b⁴. The liquid phase of FCC (Ni) starts at this temperature for amounts of combined carbon of 9.33 w% and 10 w%. Below 9.25 w%, there is slow cooling; temperatures of 1500 °C and 1100 °C result in equilibrium phases, NbC–liquid and NbC–NbNi₃, respectively. With an amount of combined carbon of 9.25–9.75 w%, when being cooled down from 1250 °C, the formation of an NbNi₃ compound occurs, and there is a pseudo-binary region NbC + FCC + NbNi₃, with a very narrow range.^{3,4} NbC_y can form sub-cubic carbides, allowing a wide range of stoichiometry of the combined carbon, from 6.5–11.8 w%, and can be adapted by stoichiometry as shown in the Nb–C binary phase diagram, **Figure 1d**.⁵

In terms of additive manufacturing, L–PBF is a promising alternative for refractory alloys where metal powders are selectively melted layer-by-layer using a computer-controlled laser beam.⁶ One advantage of the L–PBF process is the ability to manufacture components of complex shapes and small dimensions, something that

cannot be easily manufactured with the conventional process of powder metallurgy. This technology has been used more frequently by several industrial sectors in order to reduce production steps, mainly for manufacturing mechanical components with complex geometries, and with a high value and low volume of production.⁷ The present work aims to compare the microstructure characteristics and properties of NbC–30Co, NbC–30Ni and NbC–30(Co, Ni) alloys, manufactured using the conventional liquid phase sintering (LPS) process and laser powder bed fusion (L–PBF), to point out the challenges in the additive manufacturing of the cermet based on NbC with alternative binding phases.

2 EXPERIMENTAL PART

This section presents the experimental procedures including the conventional (pressing and sintering) and selective laser melting AM (L–PBF) process. The following cemented carbide samples were prepared, with the compositions shown in **Table 2**: (I) NbC–30Co, (II) NbC–30Ni and (III) NbC–30(Co, Ni). High-purity com-

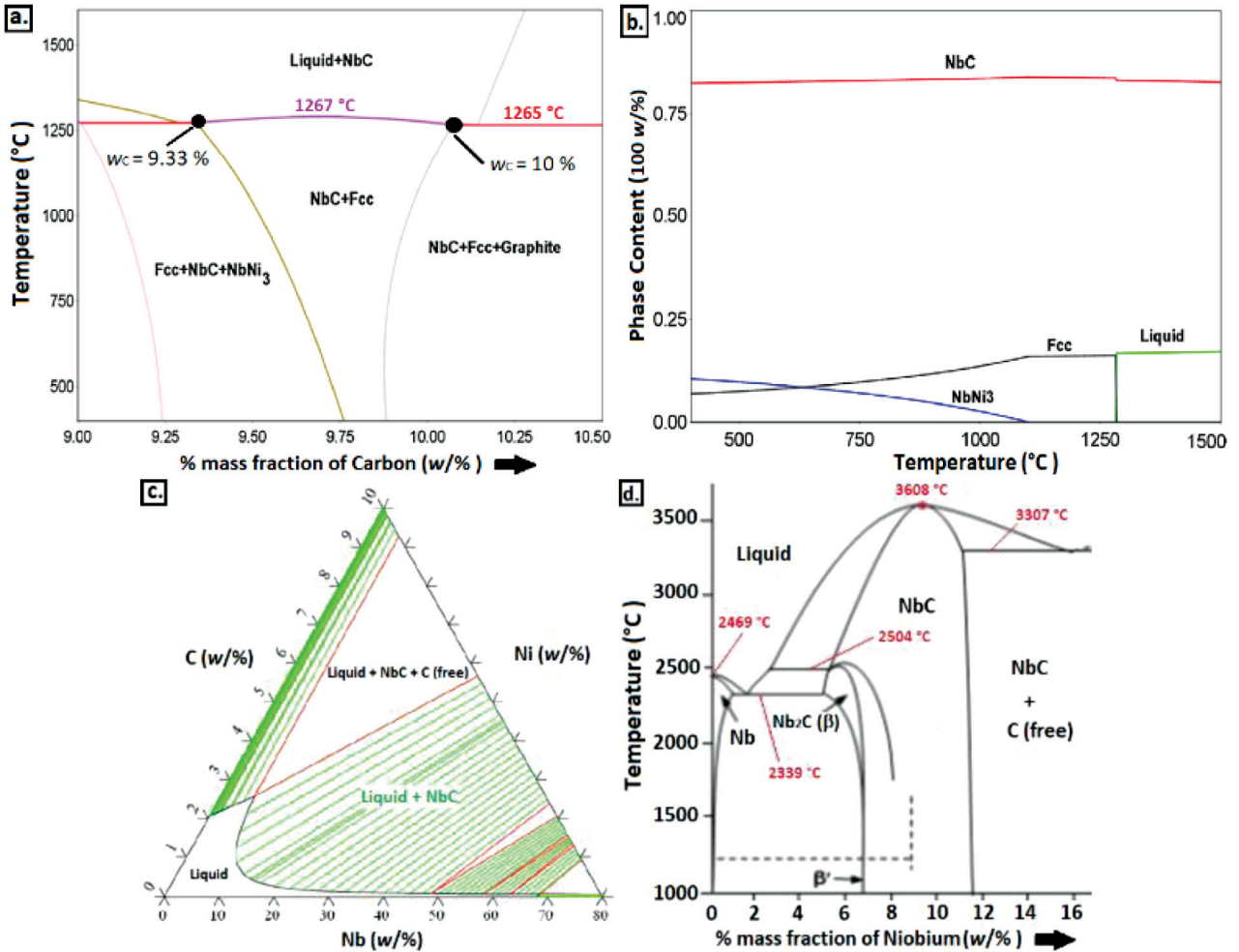


Figure 1: a) Phase evolution with temperature of the studied NbC-12Ni cermet, b) Phase diagram simulation of the NbC-12Ni system, c) Isothermal section of Nb-C-Ni at 1420 °C⁴, d) Binary Nb-C phase diagram⁵

Table 1: Properties of refractory metallic and ceramic powders

Powders	Theoretical density	Average grain size	Purity	Apparent density	Origin
	(g·cm ⁻³)	(µm)	(w/%)	(g cm ⁻³)	
NbC	7.750	< 1.0	99.650	3.0	F&X Electro-Materials Limited (China)
WC	15.630	1.5	99.530	4.0	Buffalo Tungsten Inc. (USA)
Co	8.908	2.0	99.970	2.0	Nanjing Hanrui Cobalt Co. (China)
Ni	8.900	5.0	99.850	2.5	CVMR Corporation (Canada)

Table 2: Weight balance (w/%) of the prepared alloys

Alloy	Description of cermets	w/%				Theoretical density (g·cm ⁻³)
		WC	NbC	Co	Ni	
I	NbC–30Co	3.0	67.0	30.0	0.0	8.003
II	NbC–30Ni	3.0	67.0	0.0	30.0	8.005
III	NbC–30(Co, Ni)	3.0	67.0	15.0	15.0	8.004

mercial Co, Ni and WC powders were used, with the following particle sizes: (2.0, 4.8 and 1.5) µm, respectively. The metal powders of NbC, Co, Ni and WC were mixed and homogenized by means of a conventional paddle stirrer for 2 h, using isopropyl alcohol to avoid breaking, crushing or reducing the particulates. **Figure 2** shows the SE of each mixture (**Table 2**) of the constituent powders (**Table 1**) used in this work. The LPS samples were compacted, without polymeric lubricants, into a metallic matrix with a rectangular shape of (6 × 12 × 37) mm, using a pressure of 50–125 MPa. Green compacted samples were sintered in a vacuum oven (2 × 10⁻² mbar), with sintering cycles at 1330 °C (1603 K) and 1370 °C

(1643 K) and a heating rate of 10 °C min⁻¹ (283 K/min), then stabilized for 60 min and slowly cooled inside the oven.

The L–PBF process was carried out in an OmniSint-160 machine, as shown in **Figure 3a**. In this machine, the powder bed is created by a vibrating device that has a rubber scraper ruler and a metallic roller. The rotational speed of the roller is independently controlled and should be zero. The area of the powder bed is too large (around 630 cm²), and the compaction force is applied by a 2 kg roller (19.6 N); thus, the compaction pressure is very low. This powder feeding device was developed specially for this L–PBF machine. The metallic

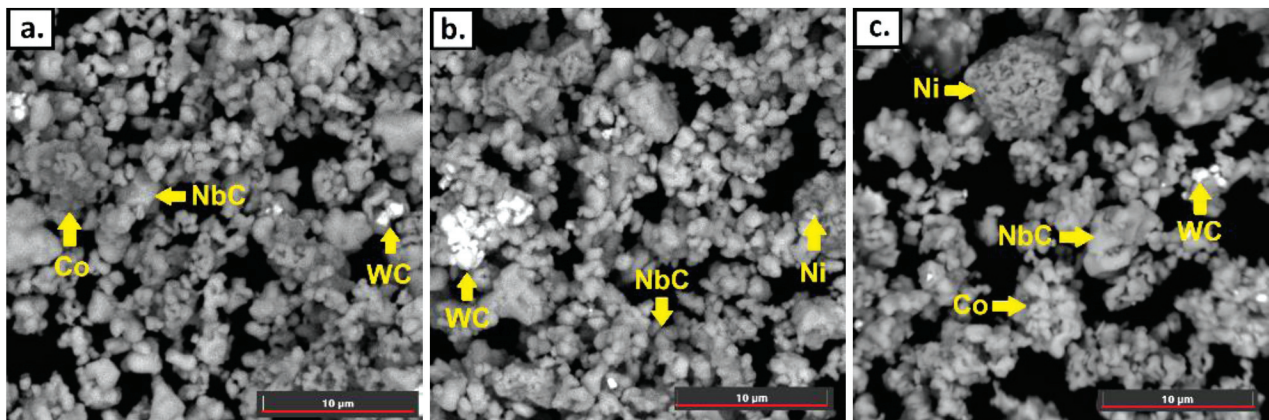


Figure 2: SE images of the mixtures of metal powders: a) (I) NbC–30Co, b) (II) NbC–30Ni and c) (III) NbC–30(Co,Ni) alloy

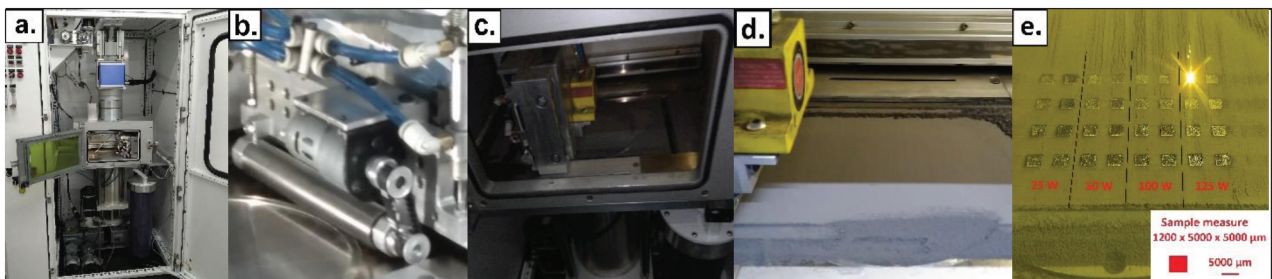


Figure 3: a) OmniSint-160 machine, b) vibration device with a roller, c) sintering chamber, d) powder bed flowability & compressibility, e) sintering with different parameter levels P_L – v_s

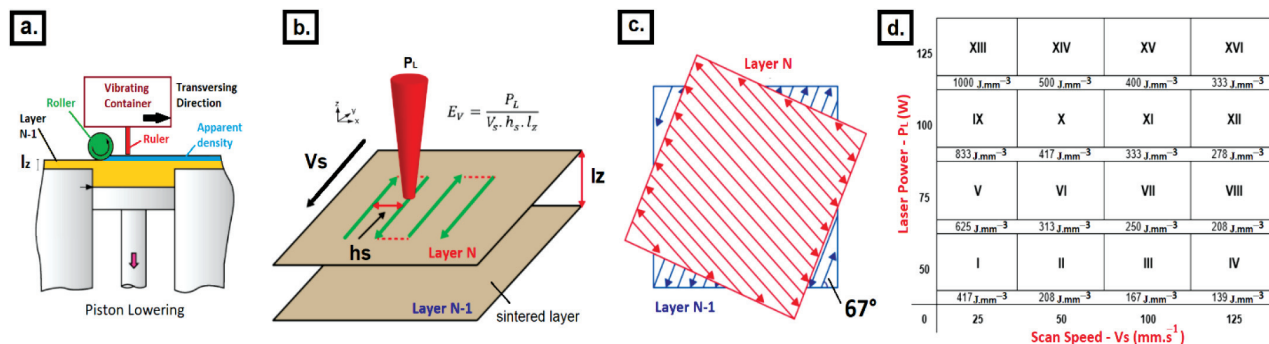


Figure 4: a) Pressing method⁸, b) Zigzag scanning strategy, c) Monolayer deposition strategy with 67° rotation, d) Sintering strategy via L-PBF, generated by different levels of factors $P_L - v_s$

powder is fed manually into a container that has a capacity of 1500 g and is vibrating. It makes the powder go through a 35 mesh sieve. The translation and rotation movement simultaneously spreads and compacts the powder, generating a powder bed, **Figure 3d**. Thin layers are produced with the rollers and it is possible there is even extra fine metal powder, used for 3D printing additive manufacturing. During direct sintering, the chamber was inertized with a high-purity dynamic argon atmosphere (0.3 L min^{-1}), **Figure 3c**. The oxygen concentration during the process was around $300 \mu\text{g/g}$. The depo-

sition was limited to 40 layers, with a layer thickness of $30 \mu\text{m}$. The shrinkage during consolidating was high, so the final sample thickness was smaller than $1200 \mu\text{m}$.

Figure 4a shows a schematic of the process parameters for L-PBF, **Figure 4b** presents a 3D view for the L-PBF process, and **Figure 4c** presents the scanning strategy with a 67° rotation, from layer N to layer N-1. The laser power (P_L) ranged from 50–125 W, the scan speed (v_s) parameter ranged from 50–150 $\text{mm}\cdot\text{s}^{-1}$, keeping the scan line spacing (h_s) equal to $80 \mu\text{m}$. The layer

T(°C)	1330 °C		1370 °C	
	Alloy (I) Co Binder Phase			
Alloy (II) Ni Binder Phase				
Alloy (III) Co-Ni Binder Phase				

Figure 5: Types of apparent porosities (ISO 4505) and microstructures (ISO 4499) of samples NbC–30Co, NbC–30Ni and NbC–30(Co, Ni) produced via the conventional LPS route ($\sigma = 125 \text{ MPa}$)

thickness (Iz) was 30 μm . The focus diameter was 140 μm .

3 RESULTS AND DISCUSSIONS

The apparent porosities (LM 100 \times) and microstructures of the samples obtained with light microscopy (LM) after the LPS process at temperatures of 1330 $^{\circ}\text{C}$ (1603 K) and 1370 $^{\circ}\text{C}$ (1643 K) are presented in **Figure 5**. During sintering, solid-solid bonding occurs between the NbC carbides, before the emergence of the liquid phase, forming necks between the particles and porosities. The Ni and Co–Ni binding phases of the samples sintered at 1370 $^{\circ}\text{C}$ indicate good wettability around the NbC grains. For the Co-based alloys, the NbC grains are not well rounded. In the NbC–Co alloy, density can be achieved in the solid-solid and solid-liquid state; however, the microstructures are not spheroidized and the mechanical properties are very low.^{3,4} Metallographic determination of the porosity and uncombined carbon was performed via LM (100 \times). The alloys manufactured via LPS at the temperature of 1330 $^{\circ}\text{C}$ show apparent porosities of types A08 and B08 (0.6 $\varphi\%$, 4000 pores cm^{-2}) and at 1370 $^{\circ}\text{C}$, they show porosities of types A02 to A06 (0.02–0.2 $\varphi\%$, (140 to 1300) pores cm^{-2}), according to ASTM B276. The γ -phase is determined after surface etching with a Murakami reagent when the phase is light yellowish-brown and has a typically rounded shape. Its size is estimated and recorded as γ -fine, γ -medium or γ -coarse according to ISO 4499. The metallographic analysis shows a good granulometric and homogeneous distribution of NbC for the NbC–30Ni and NbC–30(Co, Ni) alloys. The microhardness values (HV1) are presented in **Figure 5a** for all 3 chemical compositions, (I) NbC–30Co alloy, (II) NbC–30Ni alloy and (III) NbC–30(Co, Ni) alloys.

Figure 5 presents the microstructures of the samples sintered at 1330 $^{\circ}\text{C}$ and 1370 $^{\circ}\text{C}$. It is possible to observe, considering micrographs with a low magnification of 100 diameters (ISO 4505), that the level of porosity is particularly low for the NbC–30Ni and NbC–30(Co, Ni) samples. Micrographs with a low magnification of 1500 diameters (1 μm = 0.00003937 in) (ISO 4499) show that Ni is the best binder for NbC, providing a more homoge-

neous microstructure with a better distribution of the carbides. There are Co pools for NbC–30Co.

For the NbC–12Ni alloys, the eutectic temperature is 1265 $^{\circ}\text{C}$, **Figures 1a** and **1b**,^{3,4} while for the NbC–30Ni and NbC–30(Co, Ni) alloys, this temperature is higher, around 1350 $^{\circ}\text{C}$. Thus, alloys with nickel or cobalt-nickel should be sintered at higher temperatures, higher than the sintering temperature used here (1370 $^{\circ}\text{C}$) in order to obtain more homogeneous microstructures, with the carbide grains well dispersed in the binder phase. The hardness obtained for NbC–Co is lower than for WC–Co alloys,¹⁰ while higher values can be achieved with sintering temperatures higher than 1370 $^{\circ}\text{C}$.

The sintering of conventional WC–Co hard metals with a high content of the binder phase is carried out in a temperature range of 1300–1380 $^{\circ}\text{C}$. For this work, temperatures of 1330 $^{\circ}\text{C}$ and 1370 $^{\circ}\text{C}$ were chosen. Due to the low hardness of hard metals, depending on the binder phase (20–30 $w\%$), which varies from 600–900 HV, it is possible to carry out conventional machining of parts after sintering. The results are similar to those found in the literature for conventional cemented carbides WC–Co, showing the efficiency of obtaining the mixtures by means of weight balance.^{1–2,11–12} To obtain the Vickers microhardness (1 kgf), the values were calculated based on the ASTM C1327-15 standard, presenting the average of 10 microhardness values obtained with their respective standard deviations. **Figures 6a** to **6c** show properties of the samples sintered with LPS, as a function of the temperatures of 1330 $^{\circ}\text{C}$ and 1370 $^{\circ}\text{C}$.

The melting point of Ni equals 1455 $^{\circ}\text{C}$, which is lower than that of cobalt at 1495 $^{\circ}\text{C}$. However, for the sintered products NbC–(Co, Ni), obtained via LPS, to achieve a satisfactory densification, it is necessary to use a longer stabilization time and/or a higher temperature during the furnace LPS. The problem related to this is that nickel has a ten time greater vapor pressure than cobalt in the LPS process, which results in a considerable loss of the nickel binding phase and, therefore, it is necessary to control the working pressure. The loss of nickel in practice has been reported to range from 4–10 $w\%$, depending on the sintering temperature.¹³ It can be seen in **Table 2** that the densities of the samples sintered at

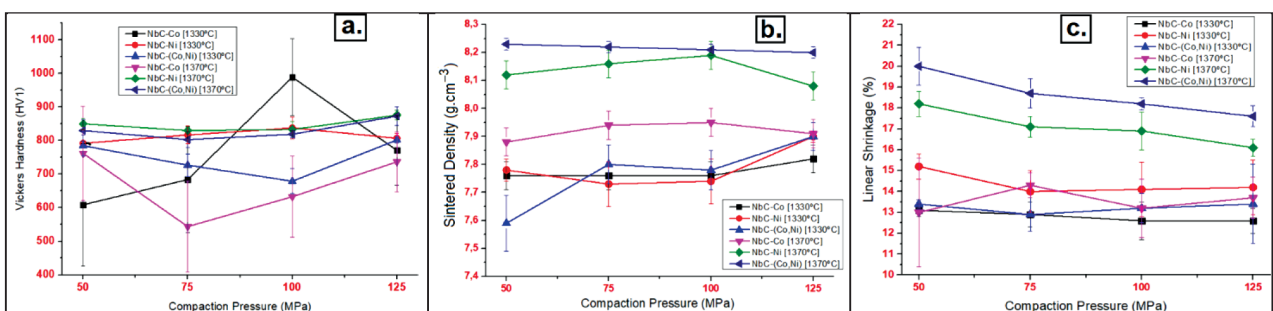


Figure 6: a) Vickers hardness (HV1), b) Density ($\text{g}\cdot\text{cm}^{-3}$), c) Linear shrinkage (%) of NbC–30Co, NbC–30Ni and NbC–30(Co, Ni) samples as a function of compaction pressures (MPa) for the temperatures of 1330 $^{\circ}\text{C}$ and 1370 $^{\circ}\text{C}$

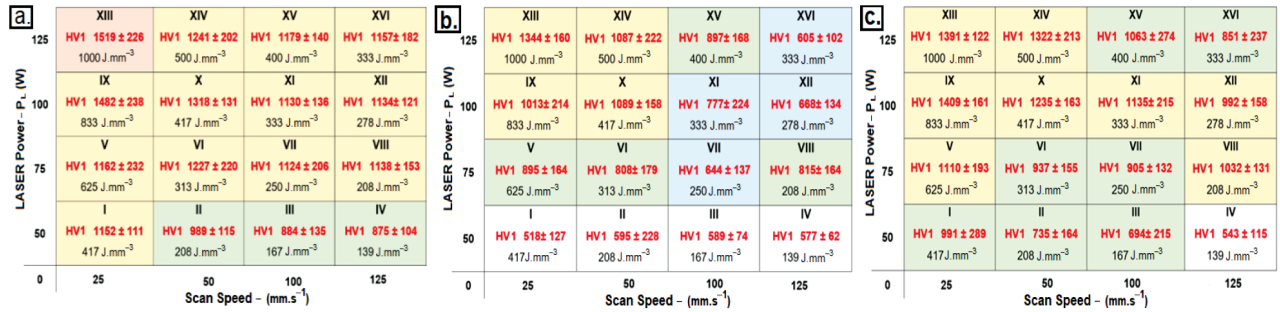


Figure 7: Microhardness characteristics of: a) NbC–30Co, b) NbC–30Ni and c) NbC–30(Co,Ni) alloys as a function of the sintering strategy using L–PBF with different factor levels (PL–vs)

1370 °C exceeded the theoretical density, making it difficult to compare the relative densities of the NbC–30Ni and NbC–30(Co, Ni) samples. However, the NbC–30Ni and NbC–30(Co, Ni) alloys showed the best linear shrinkages, from 18–20 w%, similar to those of the conventional WC–Co alloys, with high levels of the binder phase.

Among the samples processed via LPS, the NbC–30Ni alloy showed the mean microhardness values, HV 839 ± 67 (1330 °C) and HV 847 ± 21 (1370 °C), which were higher than those of alloys NbC–30Co, being HV 756 ± 150 (1330 °C) and HV 669 ± 100 (1370 °C) and NbC–30(Co,Ni), being HV 748 ± 56 (1330 °C) and HV 831 ± 30 (1370 °C), indicating that NbC–Ni hybrid particles are harder than NbC–Co particles and the alternative NbC–(Co,Ni) binding phase. Furthermore, when compared with traditional alloys, the microhardness of the NbC–30Ni alloy was higher than

the hardness of WC–Co (HV 800),¹² though this value may be overestimated. The hardness of conventional cemented carbides (hard metals) may vary from HV30 1000–2000 with the cobalt content varying from 10–20 w% for submicrograins (< 1 µm) and fine grains (> 2 µm), respectively.¹⁴ For NbC-based cermets with a high level of binder phase, 20 w%, the Vickers microhardnesses should vary from HV30 900–1100, depending on the average grain size of NbC and the addition of WC as the reinforcement to the metallic matrix.⁵ For WC-Co traditional alloys, the hardness ranges from HV 800–2000^{11,12} with the WC constituent ranging from 75–95 w% and the Co content ranging from 5–25 w%. These are produced with conventional molding methods, including injection molding, extrusion molding and powder metallurgy.^{11,12}

Investigations of the L–PBF process (direct sintering) included the creation of a PL(W)–vs(mm.s⁻¹) process

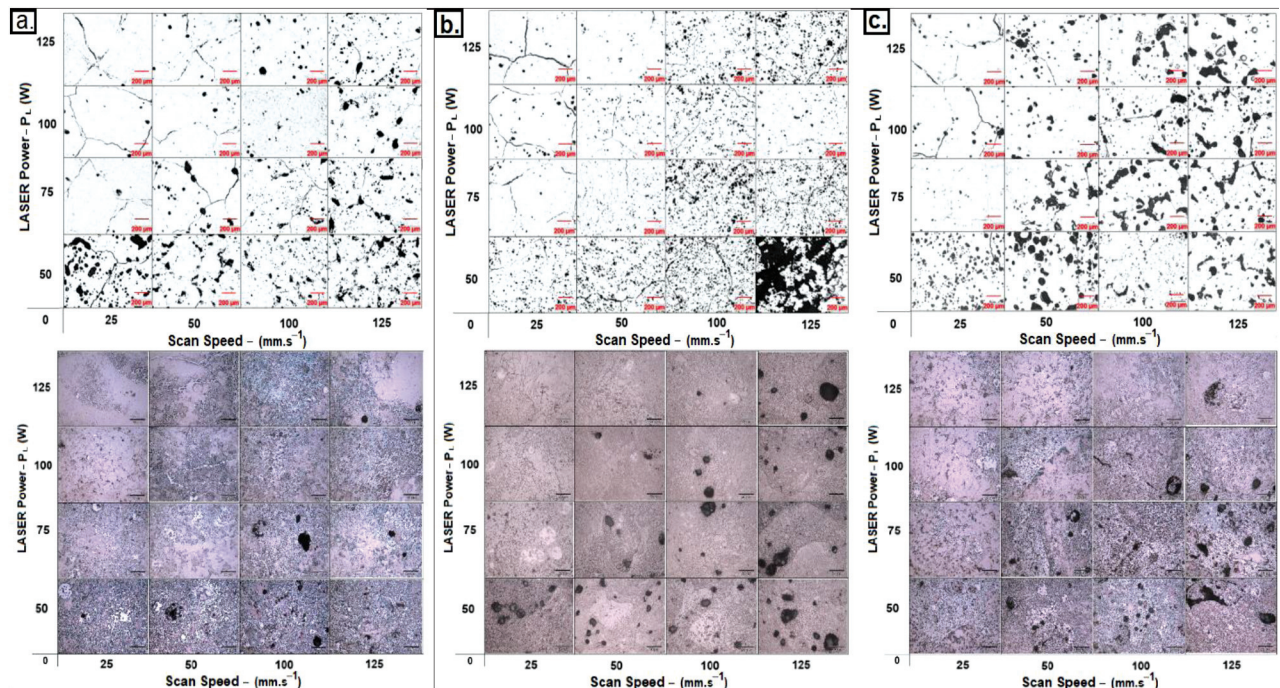


Figure 8: Apparent porosity, 140–4000 pores·cm⁻², (100×) and microstructure of samples (LM 1000×): a) NbC–Co, b) NbC–Ni, c) NbC–(Co, Ni) for different factor levels (PL–vs)

map, see **Figure 4d**, resulting in different hardness values for different energy levels ($J\cdot mm^{-3}$), **Figure 7**. **Figures 7a to 7c** show the microindentation hardness behavior of the NbC–30Co, NbC–30Ni and NbC–30(Co,Ni) alloys as a function of the sintering strategy using PBF-L for different factor levels (P_L –Vs).⁹ For this reason, a load of 1 kgf was used for comparison with the samples sintered via the conventional route, **Figure 6a**. It can be seen that in **Figure 7** the following colors were used in the tables: white, blue, green, yellow and red, correlating and differentiating the behavior of the microhardness of each sample of each group, based on previous experience, catalogs of manufacturers and researchers of traditional cemented carbide alloys.^{3,5,9,12}

In **Figure 7**, the white color indicates an application for hot forming tools, with a microhardness lower than HV 600 (< 80 HRA), a binder content of 30–35 w% and the average size of extra coarse grains (> 10 μm). The blue color indicates an application for rolls and cylinders for lamination, with a microhardness ranging from HV 600–800 (80–83 HRA), with a binder content of 25–30 w% and the average grain size ranging from coarse to extra coarse (8–10 μm). The green color indicates an application for mechanical cold forming tools and die cutting tools for thin and medium sheets, with a microhardness ranging from HV 800–1000 (83–86 HRA), with a binder content of 18–23 w% and the average grain size ranging from medium to coarse (5–7 μm). The yellow color indicates an application for wear resistant parts or components, with a microhardness ranging from HV 1100–1400 (87–90 HRA), with a binder content of 10–15 w% and the average grain size ranging from fine to medium (2–4 μm). And finally, the red color indicates an application for inserts or machin-

ing inserts, with a microhardness ranging from HV 1500–2000 (90–94 HRA), with a binder content of 3–12 w% and the average grain size ranging from sub-micron to fine (<1 μm). The relationship of the size and distribution of the apparent average grain size and metallographic determination of the microstructure in cemented carbides, for each application cited above, are based on ASTM B 390 and ISO 4499 standards. When selecting the compositions of refractory alloys based on NbC, or WC, and suitable processing parameters (LPS and L-PBF process) for hard metals, a wide combination of mechanical properties can be achieved. In particular, their combination of microhardness and toughness make them attractive for many industrial applications.¹² However, the variation in the binder content, carbide particle size and carbide particle distribution are critical factors that affect the mechanical properties of cermets, mainly the hardness values.¹¹

Figure 8 shows the porosity, cracks and microstructures (observed with the LM) of the NbC–30Co, NbC–30Ni and NbC–30(Co, Ni) samples produced with L–PBF. To visualize the porosities and cracks of the samples, the LM with a 100 \times magnification without a chemical etch was used. To reveal the microstructures, an electrochemical etch produced with a Murakami instrument was used at 3 V for 5 s. The hypotheses about the cracks, or embrittlement, of some samples may be related to the loss of the combined carbon content due to the presence of oxygen during sintering, detected by a gas sensor (300 $\mu g/g$), resulting in the formation of compounds, or brittle phases, and residual stresses during cooling. In addition, the evaporation of the binder phase occurs, which consequently decreases the size of the NbC grains and forms embrittlement compounds; for ex-

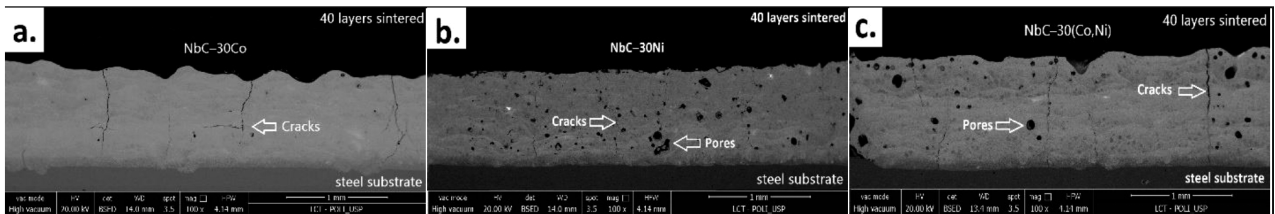


Figure 9: Sample XIII ($1000 J\cdot mm^{-3}$) section in the building direction bottom up: a) NbC–30Co alloy, b) NbC–30Ni alloy and c) NbC–30(Co,Ni) alloy

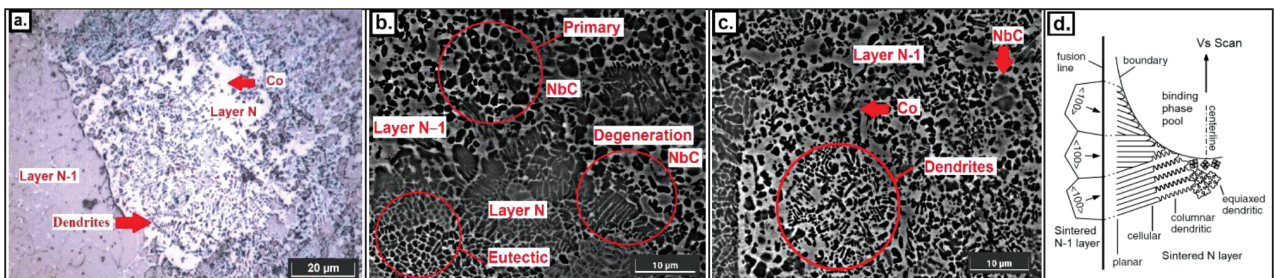


Figure 10: a) LM (1500 \times), b) SEM (5000 \times) sintered region N-1 layer, c) SEM (5000 \times) sintered region N layer of NbC–30Co sample X; $P_L = 100 W$, $v_s = 50 mm\cdot s^{-1}$, $E_v = 417 J\cdot mm^{-3}$, d) Schematic model of equiaxed dendritic solidification across the fusion zone and constitutional supercooling in the solidification mode during L–PBF

ample, for the NbC–30Ni alloy, there is a high probability for the formation of NbNi₃ and Nb₂C compounds or phases, **Figures 1a** and **1d**⁴, due to the carbon loss and Ni evaporation, as well as an abnormal NbC grain growth, **Figures 8a** to **8c**, seen in the microstructures of cermets obtained via L–PBF, especially for the Ni-based alloys above 330 J·mm⁻³. The formation of embrittlement phases in the NbC-based alloys, at specific points in the samples, is related to the loss of carbon, **Figure 1d**, due to the high energy involved in the L–PBF process. The presence of oxygen inside the sintering chamber contributes to the loss of carbon, which depends on the atmosphere during direct sintering and, therefore, the carbon mass balance cannot be fully controlled, decarburization is inevitable and, consequently, there are variations in the hardness for different energy levels. Moreover, uncertainties arise in the control of the microstructures, regarding the ternary phase diagrams of NbC alloys.¹⁵ The NbC–30 Ni and NbC–30(Co, Ni) alloy samples showed smaller amounts of microcracks when compared to the NbC–30Co alloy. However, they also showed the highest amount of macroporosity. The cracks may be related to the high thermal gradient and porosity with a combination of the power and scanning velocity of the laser beam. NbC particles are directly exposed to a laser beam, and due to the excess energy, they can melt and grow abnormally.

The NbC–30Co alloy samples showed higher hardness values compared to the NbC–30Ni and NbC–30(Co, Ni) samples, for all energy levels (J·mm⁻³). All samples number XIII (1000 J·mm⁻³) of the NbC–30Co, NbC–30Ni and NbC–30(Co, Ni) alloys, **Figures 9a** to **9c**, respectively, were, in general, apparently dense, but microcracks and porosities of type A and B, from 10–25 µm, were observed. It was not possible to determine experimental densities because samples were very small (< 1 µm), and with irregular shapes and surfaces. We detected porosities and microcracks of the samples with different chemical compositions (NbC–30Co, NbC–30Ni and NbC–30(Co, Ni)), produced with the same volumetric energy density (1000 J·mm⁻³). Porosity was lower for NbC30Co, probably due to a better interaction of liquid Co with NbC particles. On the other hand, microcracks are related to high thermal gradients. The L–PBF samples had 40 layers; as I_z was 30 µm, the expect thickness was 1200 µm. The average printed thickness was 802 ± 65 µm, so the shrinkage was 33.2 ± 6 %.

The microstructure obtained with the L–PBF process showed dendrites and abnormal growth of NbC for all samples, **Figures 10a** to **10c**. In the LPS process, the redistribution of solute in the liquid and in the solid have the values predicted by the phase diagrams, but this only occurs with very slow cooling. However, using the L–PBF process, this does not occur under normal solidification conditions. These out-of-equilibrium conditions tend towards high microsegregation, emergence of den-

drites Ni₃Nb and NbC abnormal grain growth. **Figure 10d** shows the solidification mode from the plane to the cell for the NbC-based carbide alloys. The effect of constitutional supercooling on the solidification mode makes it columnar dendritic and equiaxed dendritic. The greater the constitutional supercooling in the binding phase, the easier is the nucleation of columnar grains and equiaxed dendrites.¹⁶ According to the classical theory of eutectic growth, the growth, or solidification rate, and the thermal gradient at the solid/liquid interface are fundamental parameters for defining the solidification microstructure.

The obtained microstructures are evaluated with regard to their regularity and dimensions, and also in relation to the formation of primary NbC phases, NbC precipitations and the degeneration of the eutectic structure. The microstructural analysis of the samples processed via L–PBF with a varied thermal gradient and different growth rates revealed three distinct types of microstructure: eutectic-rich regions, columnar and equiaxed dendrites. We noticed the limitation of the magnification in the case of LM and the identification of microconstituents when compared with SEM, mainly when observing the interface of layer N–1 with layer N, **Figures 10a** and **10c**. The existence of this coarse region in the contours, **Figures 10 b**, indicates that there was solute segregation, necessary to adjust the volume fractions of the phases. The formation of a cellular microstructure or eutectic regions is associated with a combined effect of the impurities rejected from the solid phases, the growth rate and the thermal gradient imposed on the solid/liquid interface, resulting in constitutional supercooling ahead of the interface.

4 CONCLUSIONS

In summary, the main objective of this work was to compare the microstructures, porosities and hardness of the NbC–30Co, NbC–30Ni and NbC–30(Co, Ni) alloys obtained via LPS and L–PBF sintering processes. From the results obtained, the following conclusions are drawn:

- The solidification microstructures of cermet alloys obtained via L–PBF are very dependent on the temperature, energy and mainly on the cooling rate, with which the crystallographic orientation and morphology of NbC can be modified easily when compared to the LPS technique.
- All alloys obtained via L–PBF showed dendritic structures and an abnormal grain growth of NbC. At higher rates ($E_v > 400$ J·mm⁻³), they transformed into heterogeneous microstructures, with regions rich in eutectic, columnar dendritic and equiaxed dendritic growth.
- The NbC–Ni and NbC–(Co, Ni) alloys obtained via LPS showed complete densification and a regular microstructure when compared with the NbC–Co al-

loy samples at 1370 °C kept in a vacuum oven for 60 min.

- The abnormal growth of NbC grains was due to dissolution and reprecipitation into larger NbC grains. The alloys containing the Co binder phase showed a higher hardness when compared to those containing Ni and Co-Ni.
- The indentation microhardness obtained via L-PBF increases due to a higher power and lower scanning speed of the laser and it is superior to the samples processed via LPS, with energies above 400 J·mm⁻³.
- Samples with high energy (Ev > 400 J·mm⁻³) exhibited irregular microstructures, high hardness and microcracks. Samples with low density energies (Ev < 300 J·mm⁻³) exhibited regular microstructures, but with microporosity, a lack of binder phase and a lack of fusion between the layers of deposition.

Acknowledgment

The authors thank *Fundação de Amparo Pesquisa do Estado de São Paulo* (FAPESP), Brazil, Process number: 2022/06201-7, linked to the Process: 2019/08927-2, for the financial support.

5 REFERENCES

- ¹ M. Labonne, J.-M. Missiaen, S. Lay, N. García, O. Lavigne, Sintering behaviour and microstructural evolution of NbC–Ni cemented carbides with Mo₂C additions, *International Journal of Refractory Metals & Hard Materials*, (2020), <https://www.sciencedirect.com/science/article/am/pii/S0263436820301712>
- ² A. S. Kurlov, A. I. Gusev, Density and particle size of cubic niobium carbide NbC_y nanocrystalline powders, *Physics of the Solid State*, 59 (2017) 1, 176–182, doi:10.21883/FTT.2017.01.43971.182
- ³ D. Rodrigues, E. Cannizza, The use of NbC₂₀Ni hard materials for hot rolling applications, *Proc. of the 19th Plansee Seminar, International Conference on Refractory and Hard Materials, 2017, Reutte, Austria, HM59*
- ⁴ S. G. Huang, P. De Baets, J. Sukumaran, H. Mohrbacher, M. Woydt, J. Vleugels, Effect of Carbon Content on the Microstructure and Mechanical Properties of NbC–Ni Based Cermets, *Metals*, 8 (2018) 3, 178, doi:10.3390/met8030178
- ⁵ L. J. Fernandes, R. L. Stoeterau, G. F. Batalha, D. Rodrigues, A. V. Borille, Influence of sintering condition on the tool wear of NbC-based Ni binder-cemented carbide cutting tools, *Int. J. Adv. Manuf. Technol.*, 106 (2020), 3575–3585 doi:10.1007/s00170-019-04838-0
- ⁶ J. Li, Z. Wei, B. Zhou, Y. Wu, S.-G. Chen, Z. Sun, Densification, Microstructure and Properties of 90W-7Ni-3Fe Fabricated by Selective Laser Melting, *Metals*, 9 (2019) 8, 884, doi:10.3390/met9080884
- ⁷ A. T. Sidambe, Y. Tian, P. Prangnell, P. Fox, Effect of processing parameters on the densification, microstructure, and crystallographic texture during the laser powder bed fusion of pure tungsten, *International Journal of Refractory Metals and Hard Materials*, 78 (2019), 254–263, doi:10.1016/j.ijrmhm.2018.10.004
- ⁸ T. Niino, K. Sato, Effect of Powder Compaction in Plastic Laser Sintering Fabrication, (2009) doi:10.26153/tsw/15100
- ⁹ E. Uhlmann, A. Bergmann, W. Gridin, Investigation on Additive Manufacturing of Tungsten Carbide-cobalt by Selective Laser Melting, *Procedia CIRP*, 35 (2015), 8–15, doi:10.1016/j.procir.2015.08.060
- ¹⁰ N. Al-Aqeeli, N. Saheb, T. Laoui, K. Mohammad, The synthesis of nanostructured WC-based hardmetals using mechanical alloying and their direct consolidation, *Journal of Nanomaterials*, 2014 (2014), 1–16, doi:10.1155/2014/640750
- ¹¹ Y. Yang, C. Zhang, D. Wang, L. Nie, D. Wellmann, Y. Tian, Additive manufacturing of WC-Co hardmetals: a review, *Int. J. Adv. Manuf. Technol.*, 108 (2020), 1653–1673, doi:10.1007/s00170-020-05389-5
- ¹² J. García, V. Collado Ciprés, A. Blomqvist, B. Kaplan, Cemented carbide microstructures: A review, *International Journal of Refractory Metals and Hard Materials*, 80 (2019), 40–68, doi:10.1016/j.ijrmhm.2018.12.004
- ¹³ C. M. Fernandes, A. M. R. Senos, Cemented carbide phase diagrams: A review, *Int. Journal of Refractory Metals and Hard Materials*, 29 (2011), 405–418, doi:10.1016/j.ijrmhm.2011.02.004
- ¹⁴ C. Liu, Alternative binder phases for WC cemented carbides, Master Thesis KTH, School of Industrial Engineering and Management (ITM), Materials Science and Engineering, (2014), 121, <https://api.semanticscholar.org/CorpusID:137038835>
- ¹⁵ S. W. Lee, Y. W. Kim, K. M. Jang, J. W. Lee, M.-S. Park, H. Y. Koo, G.-H. Ha, Y. C. Kang, Phase control of WC-Co hardmetal using additive manufacturing technologies, *Powder Metallurgy*, 65 (2021) 1, 13–21, doi:10.1080/00325899.2021.1937868
- ¹⁶ S. Kou, *Welding Metallurgy*, Hoboken, NJ, USA, John Wiley & Sons, Inc., 2002, doi:10.1002/0471434027